catalysts

MDPI

Article

Support Screening Studies on the Hydrogenation of Levulinic Acid to γ-Valerolactone in Water Using Ru Catalysts

Anna Piskun, Jozef G. M. Winkelman, Zhenchen Tang and Hero Jan Heeres *

Chemical Engineering Department, Engineering and Technology Institute Groningen (ENTEG), University of Groningen, Nijenborg 4, 9747 AG Groningen, The Netherlands; a.s.piskun@rug.nl (A.P.); j.g.m.winkelman@rug.nl (J.G.M.W.); z.tang@rug.nl (Z.T.)

* Correspondence: h.j.heeres@rug.nl; Tel.: +31-50-363-4174; Fax: +31-50-363-4479

Academic Editors: Albert Demonceau, Ileana Dragutan and Valerian Dragutan

Received: 21 June 2016; Accepted: 17 August 2016; Published: 30 August 2016

Abstract: γ-Valerolactone (GVL) has been identified as a sustainable platform chemical for the production of carbon-based chemicals. Here we report a screening study on the hydrogenation of levulinic acid (LA) to GVL in water using a wide range of ruthenium supported catalysts in a batch set-up (1 wt. % Ru, 90 °C, 45 bar of H_2, 2 wt. % catalyst on LA). Eight monometallic catalysts were tested on carbon based(C, carbon nanotubes (CNT)) and inorganic supports (Al_2O_3, SiO_2, TiO_2, ZrO_2, Nb_2O_5 and Beta-12.5). The best result was found for Ru/Beta-12.5 with almost quantitative LA conversion (94%) and 66% of GVL yield after 2 h reaction. The remaining product was 4-hydroxypentanoic acid (4-HPA). Catalytic activity for a bimetallic RuPd/TiO_2 catalyst was by far lower than for the monometallic Ru catalyst (9% conversion after 2 h). The effects of relevant catalyst properties (average Ru nanoparticle size, Brunauer-Emmett-Teller (BET) surface area, micropore area and total acidity) on catalyst activity were assessed.

Keywords: levulinic acid hydrogenation; γ-valerolactone; Ru-catalysts

1. Introduction

The conversion of biomass into platform molecules with a broad application range has attracted a great deal of attention in the last decade [1]. One of the interesting and promising examples of a platform molecule is γ-valerolactone (GVL). It has a large potential application range, including the use as solvent, intermediate in fine chemicals synthesis and as a fuel (additive). In addition, GVL may serve as a starting material for a number of interesting (bulk) chemicals (adipic acid, and pentanoic acid).

An efficient method for the synthesis of GVL involves the catalytic hydrogenation of levulinic acid (LA). The latter can be obtained by the dehydration of C6-sugars in acidic media [2,3]. The catalytic hydrogenation of LA is proposed to involve a two-step sequence: a metal-catalyzed hydrogenation of LA to 4-hydroxypentanoic acid (4-HPA), followed by an acid-catalyzed intra-molecular esterification to GVL (Scheme 1).

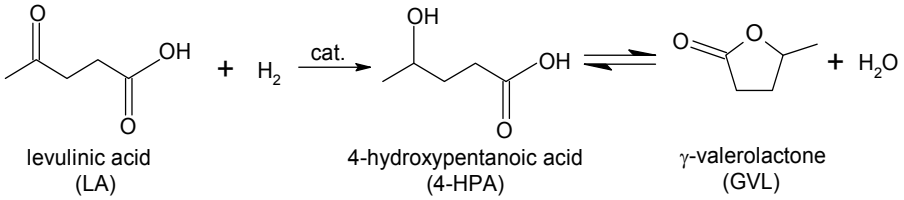

Scheme 1. Reaction scheme for the catalytic hydrogenation of LA (levulinic acid) to GVL (γ-valerolactone).

Extensive research has been performed on the hydrogenation of LA to GVL using homogeneous and (mostly) heterogeneous catalysts [2,4]. Especially, supported metal catalysts have received high attention. Manzer [5] screened the catalytic activity of Ir, Rh, Pd, Ru, Pt, Re and Ni supported on activated carbon (5 wt. %) and showed that Ru was among the most active and selective for GVL formation.

Most studies involve the use of Ru on a carbon support in various solvents (among others water, dioxane, alcohols, dimethyl sulfoxide (DMSO), and various solvent combinations) and excellent yields of GVL have been reported (>99%, Table 1). Water is the most environmentally friendly and easily available solvent for the reaction and a number of studies have been reported in water [6–8].

Table 1. Literature overview on LA (levulinic acid) hydrogenation in batch set-ups using carbon-supported ruthenium catalysts.

Catalyst	Additives	Solvent	T (°C)	H_2 (Bar)	Time (h)	LA Conversion (%)	GVL Selectivity(%)	Reference
Ru/C (5 wt. % Ru)	-	dioxane	150	55	2	80	92	[5]
Ru/C (5 wt. % Ru)	-	H_2O methanol ethanol 1-butanol dioxane methanol + H_2O ethanol + H_2O butanol + H_2O	130	12	2.7	99.5 99 76 49 99 96 99 99	86.6 85 81 82 98 88 90 76	[6]
Ru/C (3 wt. % Ru)	-	H_2O	90	45	1	100	98	[8]
$Ru_{0.9}Ni_{0.1}$/OMC (0.56 wt. % Ru 0.08 wt. % Ni)	-	H_2O	150	45	2	99	97	[9]
Ru/C (5 wt. % Ru)	-	H_2O	180	30	12	100	57	[10]
Ru/C (5 wt. % Ru)	-	H_2O (0.08 wt. %)	130	20.6	49.5	51	>99	[11]
Ru/C (5 wt. % Ru)	- A 70 [a]	H_2O	70	30	3	48 100	98 99	[12]
Ru/C (5 wt. % Ru)	-	methanol	130	12	2.7	92	99	[13]
Ru/C (5 wt. % Ru)	-	methanol 1-butanol benzaldehyde DMSO dioxane	130	12	2.7	93 0 0 0 4	99 0 0 0 0	[14]
Ru/Starbon (5 wt. % Ru)	-	ethanol + H_2O	100	10	2.2	>99	<5	[15]
Ru/C, (5 wt. % Ru)	[BMIm-SH][HSO_4] A 15 SO_4-ZrO_2	methanol	130	34.5	2	99 99 99	68 14 18	[16]

[a] A = Amberlyst.

For Ru/C, slow though irreversible deactivation was observed in water, due to Ru sintering and a reduction in the BET surface area due to coke deposition [17–19]. Other forms of carbon, like carbon nanotubes and few-layer graphene (FLG), have also been identified as promising support materials for many metal catalysts [20–22]. Advantages of CNTs as a support compared to active carbons are a higher catalyst stability and lower intra-particle diffusion limitations of reactants [23]. For LA hydrogenations in water, iridium nanoparticles supported on CNT were examined at mild reaction conditions (50 °C and 20 bar of hydrogen) resulting in excellent performance with quantitative LA conversion and 99% GVL selectivity within 1 h [20]. In the same study, ruthenium nanoparticles on CNT resulted in 65% LA conversion with 100% GVL selectivity. Graphene is a promising catalyst support due to its excellent thermal and chemical stability and high surface area. The ability of Ru/FLG (2 wt. %) to catalyze LA hydrogenation to GVL was recently demonstrated [22]. In this study, quantitative LA conversion with 100% GVL selectivity was obtained in water at room temperature (40 bar H_2, 12 h). The catalyst showed stable performance for five successive batch runs at the same reaction conditions.

Inorganic oxides (SiO_2, Al_2O_3, Nb_2O_5, ZrO_2, and TiO_2) have also been tested as a support for LA hydrogenation with Ru as the active metal (Table 2). One of the major advantages of inorganic oxides as a support is the possibility for oxidative catalyst regeneration due to their high stability at oxidative decoking conditions. However, for some of the supports (Al_2O_3 and SiO_2), the stability at hydrothermal conditions, particularly at elevated temperatures and acidity, is known to be limited, which is of relevance for LA hydrogenations carried out in water [6,24]. TiO_2 and ZrO_2 seem to be very promising supports, as was evident from a study by Lange et al. [25].

Table 2. Literature overview on LA hydrogenation in batch set-ups using supported ruthenium catalysts (excluding carbon).

Catalyst	Additives	Solvent	T (°C)	H_2 (Bar)	Time (h)	LA Conversion (%)	GVL Selectivity (%)	Reference
Ru/SiO_2 (5 wt. % Ru)	-	ethanol ethanol + H_2O	130	12	2.7	83 98	93 77	[6]
Ru/Al_2O_3 (5 wt. % Ru)	-	ethanol ethanol + H_2O	130	12	2.7	38 95	86 80	[6]
Ru/TiO_2 (Rutile) (5 wt. % Ru)		ethanol ethanol + H_2O	130	12	2.7	0 0	- -	[6]
Ru/TiO_2 (P25) (5 wt. % Ru)		ethanol ethanol + H_2O	130	12	2.7	68 81	92 88	[6]
Ru/TiO_2 (1 wt. % Ru)	-	H_2O THF	70	50	1	99 0	95 0	[7]
Ru/Nb_2O_5 (1 wt. % Ru)	-	dioxane	200	40	4	72	86	[26]
Ru/TiO_2 (1 wt. % Ru)	-	dioxane	200	40	4	100	92	[26]
Ru/Beta-12.5 (1 wt. % Ru)	-	dioxane	200	40	4	100	60	[26]
Ru/H-ZSM-5-11.5 (1 wt. % Ru)	-	dioxane	200	40	10	100	70	[27]
Ru/Al_2O_3 (5 wt. % Ru)	- A 70	H_2O	70	30	3	24 57	96 98	[12]
Ru/SiO_2 (5 wt. % Ru)	$scCO_2$	H_2O	200	100	n.a. [a]	98	> 99	[28]
Ru/Al_2O_3 (5 wt. % Ru)	$scCO_2$	-	150	145	n.a. [a]	99	99	[29]
$RuPd/TiO_2$ (1 wt. % Ru)	-	dioxane	200	40	0.5	99	99	[30]
Ru/hydroxyapatite (5 wt. % Ru)	-	H_2O ethanol ethanol + H_2O toluene	70	5	4	99 92 92 30	99 76 82 92	[31]
Ru/SPES (polyethersulfone) (2 wt. % Ru)	-	H_2O	70	30	2	88	99	[32]

[a] not available.

Zeolites have also been considered as promising supports for LA hydrogenation reactions. Luo et al. investigated the activity, selectivity and stability of ruthenium nanoparticles on strongly acidic zeolites like H-ZSM-5 and H-Beta-12.5 [26]. The reactions were carried out at elevated temperatures (40 bar H_2, 200 °C) in dioxane. Full LA conversion was achieved in both cases for 4 h reaction time but, in addition to GVL, other hydrogenation products (pentanoic acid) and corresponding esters were obtained in considerable amounts. The selectivity to GVL was around 60% for Ru/H-Beta-12.5 and around 50% for Ru/H-ZSM-5. More recently, the same group investigated the influence of the ZSM-5 cation form (H^+ versus NH_4^+), Si/Al ratio and Ru precursor on metal dispersion and acidity on product yields in LA hydrogenation [27]. The best results in terms of GVL

yield (91.6% after 10 h) were obtained using Ru/H-ZSM-5-11.5 with 1 wt. % Ru, prepared with a $RuCl_3$ precursor from the H^+ form of ZSM-5.

The one pot conversion of biomass or C6 sugars derived thereof to GVL is of high interest to eliminate an expensive separation step of the intermediate LA. It requires the use of an acid catalyst in combination with a hydrogenation catalyst. For instance, Heeres et al. have reported a one-pot synthesis of GVL from fructose using trifluoroacetic acid (TFA) and Ru/C as the catalysts [33]. A maximum GVL yield of 62 mol. % (based on fructose) at quantitative fructose conversion was obtained under optimized reaction conditions (180 °C, 94 bar H_2, 8 h). The direct synthesis of GVL from giant reed was achieved by treatment of the biomass in water with HCl and Ru/C as the catalysts [34]. Under mild reaction conditions (70 °C, 30 bar H_2, 5 h) 83 mol. % of GVL was obtained (on basis of C6 sugars in the giant reed) with full LA conversion. The use of formic acid as an acid catalyst and hydrogen source in the transformation of fructose to GVL was investigated using gold-based catalysts (150 °C, 5 h) [35]. Highest GVL yields were obtained with Au/ZrO_2 (48%) and Au/C (47%) catalysts.

On the basis of the available literature, we can conclude that a large number of supports have been tested for the hydrogenation of LA to GVL in water and organic solvents. However, a proper comparison is difficult as most studies are focused on one support only and a limited number of systematic studies with different supports is available. Recently, Abdelrahman et al. reported an experimental study on LA hydrogenation in water in a continuous packed-bed reactor using Ru on four different supports (C, SiO_2, γ-Al_2O_3 and TiO_2) [17]. The initial intrinsic hydrogenation activity was shown to be essentially independent of the support type under the prevailing conditions.

We here report an experimental study on the catalytic hydrogenation of LA with Ru based catalysts on various supports (C, CNT, SiO_2, Al_2O_3, TiO_2, ZrO_2, Nb_2O_5 and Beta-12.5) in water in a batch set-up. Reactions were performed at similar conditions, allowing for a proper comparison of catalyst performance. Catalyst activity (in terms of initial rate and turnover frequency (TOF)) and the selectivity to GVL, two important performance criteria, were determined and the best catalyst for subsequent studies was selected. In addition, relevant catalytic properties were determined and correlations between catalyst properties and performance were investigated.

2. Results and Discussion

2.1. Catalyst Characterization

All Ru-based catalysts were characterized by ammonia-TPD, N_2-physisorption and tansmission electron microscopy (TEM). In addition, the actual Ru content of the catalysts was determined by X-ray fluorescence (XRF) and inductively coupled plasma (ICP). An overview of the catalyst characterization results is presented in Table 3.

Table 3. Overview of catalyst characterization results.

Catalyst	Actual Ru Content (wt.%) [b]	Total Acidity ($\mu mol/g_{cat}$)	Type of Acid Sites	Average Ru Particle Size (TEM), (nm)	Specific Surface Area (m^2/g)	Micropore Surface Area (m^2/g)
Ru/Beta-12.5	0.97	1070	weak and medium	3.5	515	329
Ru/CNT	n.d. [c]	46	strong	1.1	272	14
Ru/C	1 [d]	99	medium	0.9	911	487
Ru/TiO_2	0.85	2.5	weak	1.4	13	0.8
Ru/SiO_2	0.71	57	weak, medium and strong	n.d.	230	9
Ru/Al_2O_3	1.2	38	weak, medium and strong	1.2	247	4.8
Ru/ZrO_2	0.71	22	weak and medium	n.d.	83	2.1
Ru/Nb_2O_5 [a]	n.d.	140	weak	n.d.	98	0

[a] ruthenium particle diameter of the Ru/Nb_2O_5 catalyst could not be determined by TEM due to lack of contrast; [b] by XRF or ICP (Ru-Beta-12.5); [c] n.d.: not determined; [d] commercial catalyst, value taken from supplier.

The Ru particle size distribution was determined by TEM and some representative images are presented in Figure 1. All catalysts showed average Ru particle sizes smaller than 2 nm, except

of Ru/Beta-12.5 (3.5 nm). Unfortunately, the average Ru particle size of Ru/Nb_2O_5 could not be determined by TEM due to lack of contrast. The average size of the Ru particles for Ru/ZrO_2 and Ru/SiO_2 were also difficult to determine accurately, though it appears that these are small and on average below 1 nm.

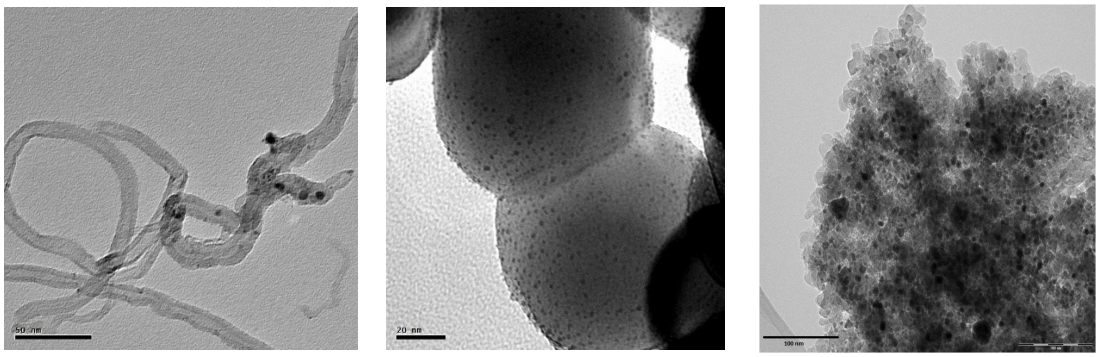

(**a**) (**b**) (**c**)

Figure 1. TEM (transmission electron microscopy) ages of: (**a**) Ru/CNT; (**b**) Ru/TiO_2; and (**c**) Ru/Beta-12.5.

The total acidity of the catalysts, as determined by ammonia TPD, span a large range and vary from 2.5 to 1070 μmol/g (Table 3). The Ru/Beta-12.5 catalyst demonstrated the highest acidity (1070 μmol/g), whereas the acidity for Ru/TiO_2 was very low (2.5 μmol/g). The acidity of Ru/TiO_2 is significantly lower than reported in the literature for P25 TiO_2, for which the total acidity is in the range of 100–300 $\mu mol/g_{cat}$ [26,36]. However, comparison is cumbersome as we used pure anatase TiO_2 in the present study. Total acidity data for pure anatase have, to the best of our knowledge, not been reported. In a recent paper, the acidic–basic properties of various TiO_2 polymorphs were evaluated by means of a TPD method using *N*-propylamine as a probe and a linear relationship between the total acidity and the BET specific surface area was demonstrated [37]. The Ru/TiO_2 catalyst used in the present study has a low specific surface area (13 m^2/g) compared to P25 (52 m^2/g), and as such a low acidity is expected, in line with the experimental data [37].

The various types of acid sites may be classified by the abundance of peaks in certain temperature ranges and are ordered as weak (<250 °C), medium (250–400 °C) and strong (>400 °C) acidic sites [38]. The results for all catalysts based on the NH_3-TPD (temperature programmed desorption of ammonia) profiles (Figure S1) are given in Table 3. Only weak acid sites were detected for the Ru/TiO_2 and Ru/Nb_2O_5 catalysts, in line with literature [26]. Medium acid sites were observed for the Ru/C catalyst, with two desorption peaks between 250 and 400 °C, in agreement with literature data for Ru/C (5 wt. % Ru) [38]. Despite the lower total acidity of Ru/CNT compared to Ru/C, the acid sites are strong in nature (compared to medium acidity for Ru/C). The acidity and type of active sites for various Ru/CNT catalysts reported in the literature varies considerably and is known to be a function of the preparation procedure (e.g., acid pre-treatment conditions) [39,40]. Weak and medium acid sites were observed for the Ru/ZrO_2 catalyst with two desorption peaks below 400 °C (Figure S1), in line with literature data [41,42]. For Ru/SiO_2 and Ru/Al_2O_3, all three types of acid sites are present. The acid sites on Ru/Beta-12.5 may be classified as weak and medium acid sites, in line with literature data [43].

The specific surface area and micropore surface area of the Ru-based catalysts were determined using N_2-physisorption and results are presented in Table 3. The highest values were observed for the Ru/C catalyst. The presence of high amount of micropores together with a high specific surface area is common for catalysts supported on activated carbon [6,17]. The specific surface area for Ru/CNT catalyst (272 m^2/g) is lower than the value for Ru/C (911 m^2/g), though in the range typically observed for multi-walled CNT (200–400 m^2/g) [44]. A high specific surface area (515 m^2/g) together with a

high micropore surface area was also observed for Ru/Beta-12.5 catalyst. Typical literature values range from 500 to 750 m^2/g, and are known to be a function of amongst others, the Si/Al ratio, nature of the cation and metal loading [26,45].

The specific surface areas of the oxide-supported ruthenium catalysts varied from 13 to 247 m^2/g. The lowest specific surface area was observed for the Ru/TiO_2 catalyst, which is on the low site compared to the specific surface areas reported for most common TiO_2 type P25 (40–60 m^2/g). This is likely due to the fact that we used the anatase phase of the catalyst, whereas P25 is a mixture of the anatase and rutile phase. The specific surface areas for the other catalysts on inorganic supports are within the ranges reported in the literature [26,46–48].

2.2. Catalytic LA Hydrogenation Experiments

Catalytic LA hydrogenation experiments were carried out in water at 90 °C, 45 bar hydrogen pressure, a stirring speed of 2000 rpm, and a LA concentration of 0.6–0.7 mol/L. The intended Ru loading on all catalysts was 1 wt. % on support, the actual loading varied between 0.71 and 1.2 wt. % (Table 3). A typical concentration profile of the reaction using Ru/C is shown in Figure 2. Full LA conversion was achieved after 4.5 h with a GVL yield of 87%, the remainder being 4-HPA. The 4-HPA concentration shows a maximum and this confirms that the hydrogenation of LA to GVL involves two-consecutive reactions, viz. the hydrogenation of LA to 4-HPA, followed by the intramolecular esterification of 4-HPA to GVL [8,49]. The latter reaction in water is known to be an equilibrium reaction, of which the equilibrium position is a function of the temperature. Subsequent hydrogenation products of GVL (methyl-tetrahydrofuran (MTHF), 1,4-pentanediol (PD), pentanoic acid etc.) were not detected for all catalytic experiments.

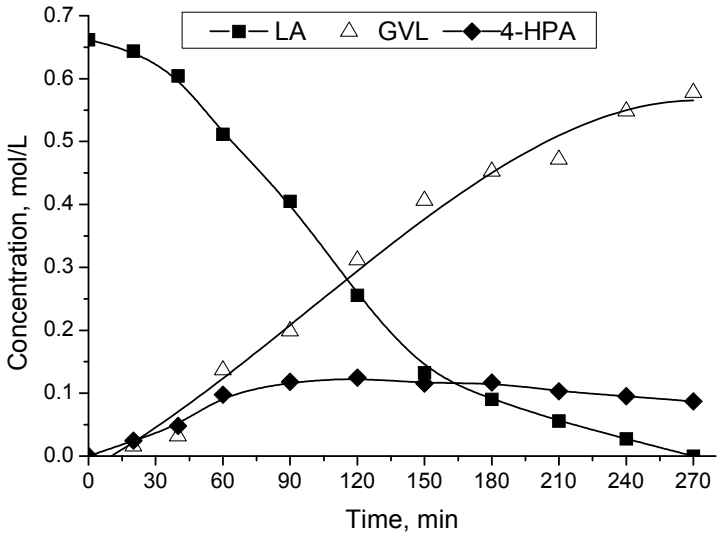

Figure 2. Typical concentrations profile for LA hydrogenation using Ru/C (1 wt. % Ru). Reaction conditions: 90 °C, 45 bar H_2, $C_{LA,0}$ = 0.6–0.7 mol/L, m_{cat} = 0.06 g, stirring rate = 2000 rpm.

A plot of the LA conversion vs. reaction time for all catalysts is shown in Figure 3 and the results are summarized in Table 4.

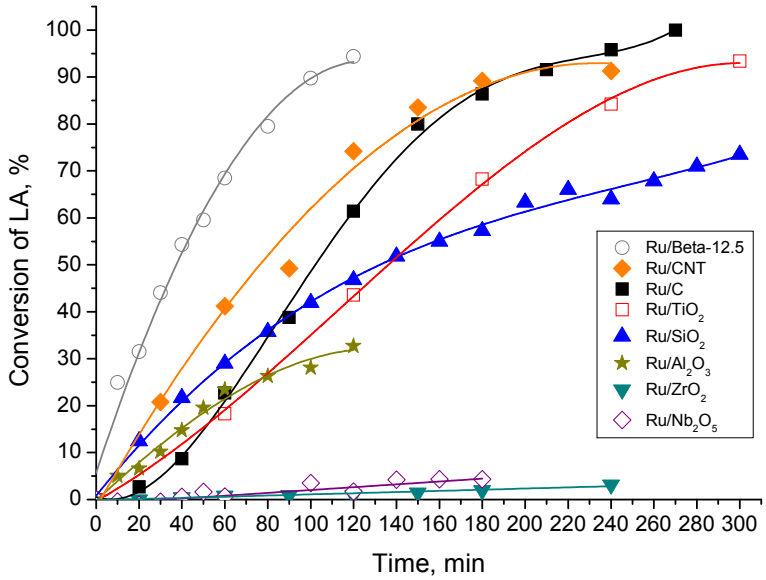

Figure 3. LA conversion in the reaction with Ru-based catalysts (1 wt. % Ru). Reaction conditions: 90 °C, 45 bar H_2, $C_{LA,0}$ = 0.6–0.7 mol/L, m_{cat} = 0.06 g, stirring rate = 2000 rpm.

Table 4. Results of LA hydrogenation reaction in presence of ruthenium-based catalysts (1 wt. % Ru) in water in a batch set-up [a].

Catalyst	X_{LA} (%)	S_{GVL} (%)	Y_{GVL} (%)	$S_{4\text{-HPA}}$ (%)	$Y_{4\text{-HPA}}$ (%)	[4-HPA]/[GVL]	R_0 ($mol_{LA}/s \cdot g_{Ru}$ [b])
Ru/C	61	77	47	23	14	0.33	5.2×10^{-3}
Ru/CNT	74	83	61	17	13	0.21	n.d. [c]
Ru/SiO_2	47	97	46	3	1	0.11	4.0×10^{-3}
Ru/Al_2O_3	33	56	18	44	14	0.79	2.4×10^{-3}
Ru/ZrO_2	1	>99	1	0	0	0	6.4×10^{-5}
Ru/Nb_2O_5	2	>99	2	0	0	0	n.d. [c]
Ru/TiO_2	44	85	37	15	7	0.18	3.8×10^{-3}
Ru/Beta-12.5	94	70	66	30	28	0.41	8.9×10^{-3}
$RuPd/TiO_2$	9	51	5	49	4	0.96	n.d. [c]

[a] Reaction conditions: 90 °C, 45 bar H_2, $C_{LA,0}$ = 0.6–0.7 mol/L, m_{cat} = 0.06 g, stirring rate = 2000 rpm, 2 h; [b] Normalized on g_{Ru} intake based on actual Ru loading of the catalyst as determined experimentally (ICP, XRF); [c] not determined.

Clear differences in catalytic activity were observed for the various catalysts, see Figure 3 for details. The most active in the series is Ru on Beta, with a 94% conversion of LA after 2 h. By far the lowest activity was found for Ru on ZrO_2 and Nb_2O_5 (<5% LA conversion) For a better comparison, the activity in terms of the LA conversion after 2 h and the initial rates of the catalyst are provided in Table 4. Here, the ratio of 4-HPA and GVL at the end of the run is also provided. Good agreement between the two catalyst activity measures (initial rate and LA conversion after 2 h) was observed (see Figure S2 (Supplementary Materials)).

When considering the carbon supports, the catalytic activity of the Ru/CNT catalyst was higher than for Ru/C at the start of the reaction, see Figure 4 for details. However, after 4 h, the LA conversion for Ru/C was slightly higher than for Ru/CNT (96% and 91%, respectively). The concentration-time profile for Ru/C shows the peculiar features of an S-shaped curve. As such the initial activity is lower than expected and this could be due to a relatively slow in-situ activation of the catalyst (e.g., by molecular hydrogen). The yield of GVL after 4 h was rather similar for both catalysts (80% and 81% respectively). Only 4-HPA was detected as an intermediate and the selectivity to both products was close to quantitative (100% for Ru/C and 99% for Ru/CNT).

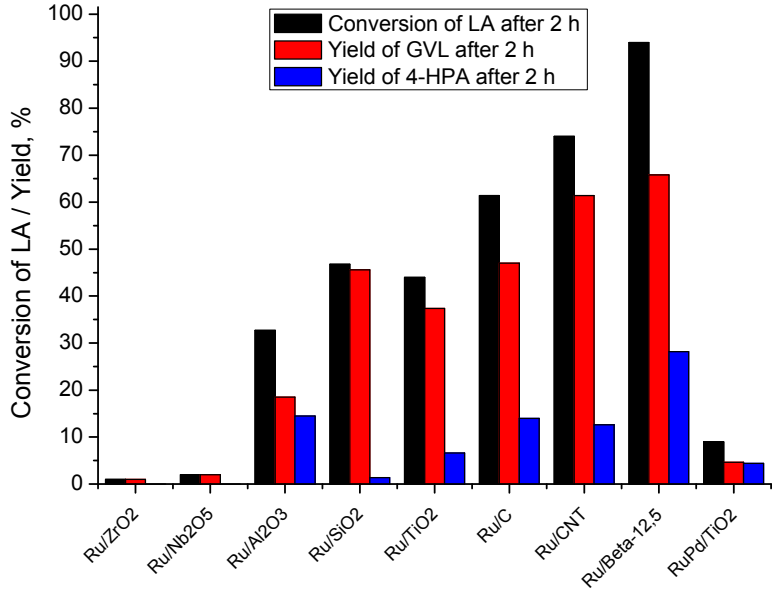

Figure 4. Conversion of LA and yield of GVL (γ-Valerolactone) and 4-HPA after 2 h batch time. Reaction conditions: 90 °C, 45 bar H_2, $C_{LA,0}$ = 0.6–0.7 mol/L, m_{cat} = 0.06 g, stirring rate = 2000 rpm.

The differences in initial rates for Ru/C and Ru/CNT may be related to the rate of catalyst activation by molecular hydrogen, which in turn is expected to be a function of the hydrogen adsorption capacity. CNTs are known for their high H_2 adsorption capacity compared to activated carbon [44]. A higher catalytic activity of metal catalysts supported on CNTs was also shown for LA hydrogenation in water for iridium catalysts [20]. H_2 temperature-programmed desorption measurements (H_2-TPD) revealed that a significantly higher amount of H_2 was desorbed from Ir/CNT compared to Ir/C. This higher hydrogen adsorption capacity for CNTs was put forward as the reason for its superior performance for LA hydrogenation to GVL [20].

When considering the inorganic supports, major differences in catalyst performance were observed. The lowest activity was found for the Ru/ZrO_2 and Ru/Nb_2O_5 catalysts and the LA conversion for these catalysts after 2 h batch time was only 1% and 2%, respectively. Improved performance was found for Ru/Al_2O_3 with 33% LA conversion after 2 h. The best results were obtained with Ru/SiO_2 and Ru/TiO_2 (47% and 44%, respectively), though the activity is less than found for Ru/C.

The best catalytic activity of the 8 catalysts tested was found for Ru-Beta-12.5. Almost full LA conversion (94%) was achieved within 2 h, compared to 4 h for Ru/C. The selectivity to 4-HPA and GVL was quantitative for both catalysts. The yield of GVL after 2 h was higher for Ru/Beta-12.5 (66%) than for Ru/C (47%), which is, among others, due to different LA conversion levels (vide infra). Good catalytic activity of this zeolite based catalyst was also demonstrated for LA hydrogenations in dioxane at 200 °C [20]. However, at these more severe reaction conditions, subsequent GVL hydrogenation products were observed, viz. pentanoic acid and pentenoic esters. At the milder reaction conditions applied in present study, over hydrogenation does not occur and only GVL and 4-HPA were observed.

Thus, it is evident that the support structure has a major impact on the activity of the catalysts and major differences in activity were observed.

2.3. LA Hydrogenation with a Bimetallic Catalyst

A recent study by Luo et al. [30] revealed positive effects of the use of bimetallic Ru based catalysts when using dioxane as the solvent, particularly when considering catalyst activity. Therefore, we have also included a bimetallic $RuPd/TiO_2$ catalyst in this catalyst screening study (Figure 5).

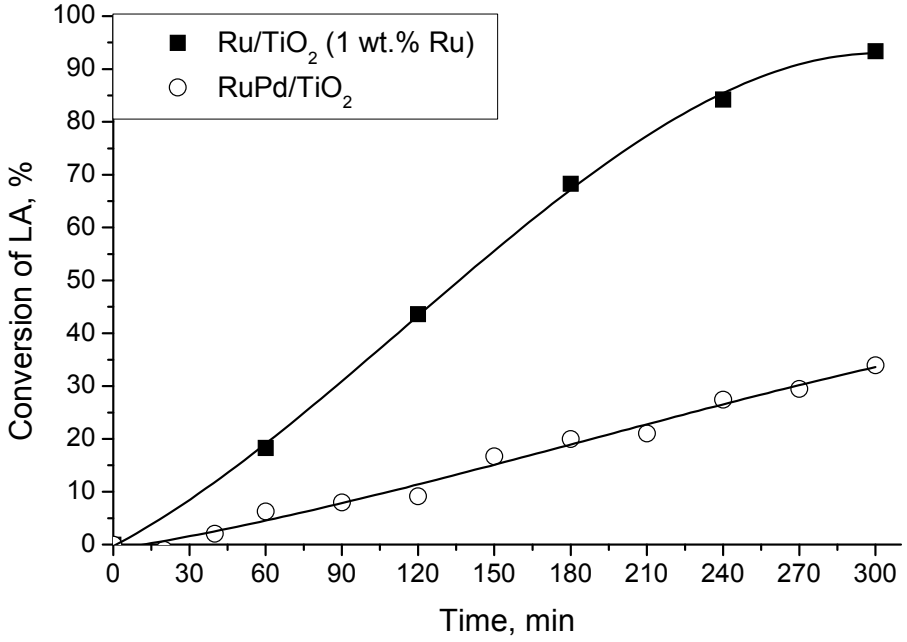

Figure 5. LA conversion versus time for the bimetallic $RuPd/TiO_2$ catalyst. Reaction conditions: 90 °C, 45 bar H_2, $C_{LA,0}$ = 0.6–0.7 mol/L, m_{cat} = 0.06 g, stirring rate = 2000 rpm.

The addition of Pd to Ru/TiO_2 resulted in a lowering of the catalytic activity. After 5 h, the LA conversion was 93% for the monometallic catalyst compared to 34% for the bimetallic catalyst. As such, the yield of GVL for the bimetallic catalyst was significantly lower (32%) than for the monometallic one (83%). In addition, the GVL to 4-HPA ratio also differed considerably for both catalysts. This reduced activity upon the addition of Pd is not in line with recent studies on LA hydrogenation in dioxane at 200 °C. Here, the bimetallic catalyst showed higher catalytic activity, stability and GVL yield than the monometallic one [30]. This was explained by considering that the active Ru sites are diluted and isolated by the introduction of Pd, resulting reduced activity for consecutive hydrogenation reactions of GVL. The lower performance in our study may be due to the use of water instead of dioxane and/or temperature effects.

2.4. Comparison of Activity of the Catalyst with Literature Data

The activity of the catalysts used in this study in terms of initial rates (R_0), together with relevant literature data, are given in Table 5. Here, only experimental data obtained in water and water-alcohol mixtures are given, as solvent effects on the catalytic hydrogenation of LA are known to be pronounced.

The reported initial rates span 3 orders of magnitude and are between 6×10^{-5} and 4.5×10^{-2} $mol_{LA}/(g_{Ru} \cdot s)$. The values reported in our study are within the ranges reported in the literature. However, a comparison is hampered as different reaction conditions and particularly different temperatures are applied in the various studies. For example, Al-Shaal reported data at 130 °C, which, as expected, resulted in higher initial reaction rate than at 70 and 90 °C [6]. However, the data do reveal some interesting trends regarding the activity of various catalysts at different temperature levels. For instance, at 130 °C, the Ru/C catalyst was shown to be more active than Ru/SiO_2, Ru/Al_2O_3 and Ru/TiO_2, and the same trend was found at 90 °C and 70 °C.

Table 5. Catalyst activity data for LA hydrogenation in water in batch set-ups.

Catalyst	wt. % Ru	T (°C)	LA Conversion after 2 h, (%)	GVL Selectivity after 2 h, (%)	4-HPA Selectivity after 2 h, (%)	R_0 ($mol_{LA}/g_{Ru} \cdot s$ [b])	Reference
Ru/C	1	90	61	75	24	5.2×10^{-3}	This study [a]
Ru/CNT	1		74	83	17	n.d.	
Ru/SiO_2	1		47	97	3	4.0×10^{-3}	
Ru/Al_2O_3	1		33	56	44	2.4×10^{-3}	
Ru/ZrO_2	1		1	99	1	6.4×10^{-5}	
Ru/Nb_2O_5	1		2	98	1	n.d.	
Ru/TiO_2	1		44	79	15	3.7×10^{-3}	
Ru/Beta-12.5	1		95	70	30	8.9×10^{-3}	
$RuPd/TiO_2$	1		9	51	49	n.d.	
Ru/C	5	130	160 min—99.5	160 min—86.6	-	3.5×10^{-4}	[6]
Ru/SiO_2	5 [c]		160 min—98	160 min—76.5	-	3.5×10^{-4}	
Ru/Al_2O_3	5 [c]		160 min—94.7	160 min—80.4	-	3.4×10^{-4}	
Ru/TiO_2	5 [c]		160 min—81.2	160 min—87.8	-	2.9×10^{-4}	
Ru/TiO_2	1	70	1 h—99%	1 h—95	-	7.9×10^{-4}	[7]
Ru/C	3	90	50 min—100%	50 min—83%	50 min—17%	4.5×10^{-2}	[8]
Ru/C	5	70	3 h—48	3 h—97.5	-	7.5×10^{-4}	[12]
Ru/Al_2O_3	5	70	3 h—24	3 h—96	-	3.7×10^{-4}	

[a] Reaction conditions: 90 °C, 45 bar H_2, $C_{LA,0}$ = 0.6–0.7 mol/L, m_{cat} = 0.06 g, stirring rate = 2000 rpm; [b] Normalized on g_{Ru} intake based on actual Ru loading of the catalyst as determined experimentally; [c] water-ethanol mixtures.

2.5. Catalyst Structure-Activity Relations

The combination of the catalytic activity data and the results from the catalyst characterization study were used to gain insights in catalyst activity-structure relations. In this case, both the initial reaction rate and the TOF values are used as activity indicator. The latter is a better measure as it is based on the amount of Ru on the surface of the nanoparticles. For calculation of the TOF values, the average Ru nanoparticle size (as determined by TEM) as well as the experimentally measured actual Ru loading are required (see Equations (1) and (2) in the experimental section for calculation details). These values are not available for all catalysts (Table 3) and as such TOF values could only be determined for four of the catalysts.

In Figure 6, the initial rate of the catalysts, both in terms of Ru intake (R_0) and TOF, is provided as a function of the average Ru-nanoparticle size. The TOF values for Ru/C, Ru/Al_2O_3 and Ru/TiO_2 are rather similar and imply that the LA hydrogenation is structure insensitive for these supports in the Ru nanoparticle size range considered here (0.9–1.5 nm). These findings are in line with data by Abdelrahman et al. for Ru catalysts on C, Al_2O_3 and TiO_2 supports [17]. However, the Ru/beta catalyst is a clear exception and by far higher TOF values are observed than for the others.

The initial rate versus the total acidity of the catalyst is given in Figure 7a. A clear correlation between initial reaction rate and total catalyst acidity is visible, with a higher support acidity leading to higher initial reaction rates. However, when plotting the TOF versus support acidity, a different trend is visible (Figure 7b). Here, the TOF is essentially independent of the total acidity for the catalysts with a low acidity (Ru/C, Ru/Al_2O_3 and Ru/TiO_2), indicative for a structure insensitive reaction, whereas the Ru/Beta-12.5 catalyst is again the clear exception.

The initial reaction rates and TOF values versus the specific surface area are given in Figure 8. The initial rate versus the specific surface area plot shows a clear maximum and the highest initial reaction rate was achieved with Ru/Beta-12.5 catalyst, which has surface area 515 m^2/g. Despite the fact that surface area of Ru/C is considerably higher, the initial reaction rate with this catalyst was significantly lower. Correlations between catalytic activity and specific surface areas have been reported for individual supports. For instance, Al-Shaal et al. reported data for titania supports with different specific surface areas and showed that high surface areas are beneficial for catalytic activity [6]. Thus, Ru/TiO_2 with a high specific surface area (48 m^2/g) gave a much higher LA

conversion (81%) and GVL yield (88%) in ethanol-water mixture than Ru/TiO_2 from Tronox (LA acid conversion below 5%), which had significantly lower specific surface area (6 m^2/g) [6].

However, it is better to compare the TOF values of the various catalysts as these are normalized on the actual amount of Ru on the surface of the nanoparticles. For Ru/C, Ru/Al_2O_3 and Ru/TiO_2, the TOF values are essentially independent of the specific surface area, whereas the Ru/Beta-12.5 catalyst is again the exception.

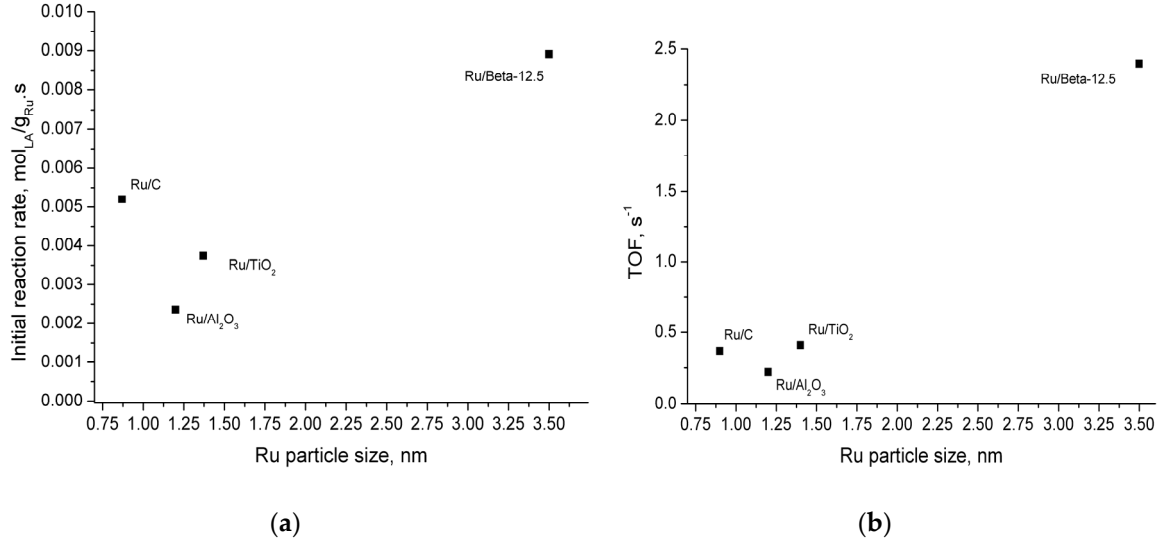

(**a**) (**b**)

Figure 6. Initial reaction rates and TOF (turnover frequency) values versus Ru particle size for LA hydrogenations using supported Ru catalysts. (**a**) Initial reaction rate, (**b**) TOF.

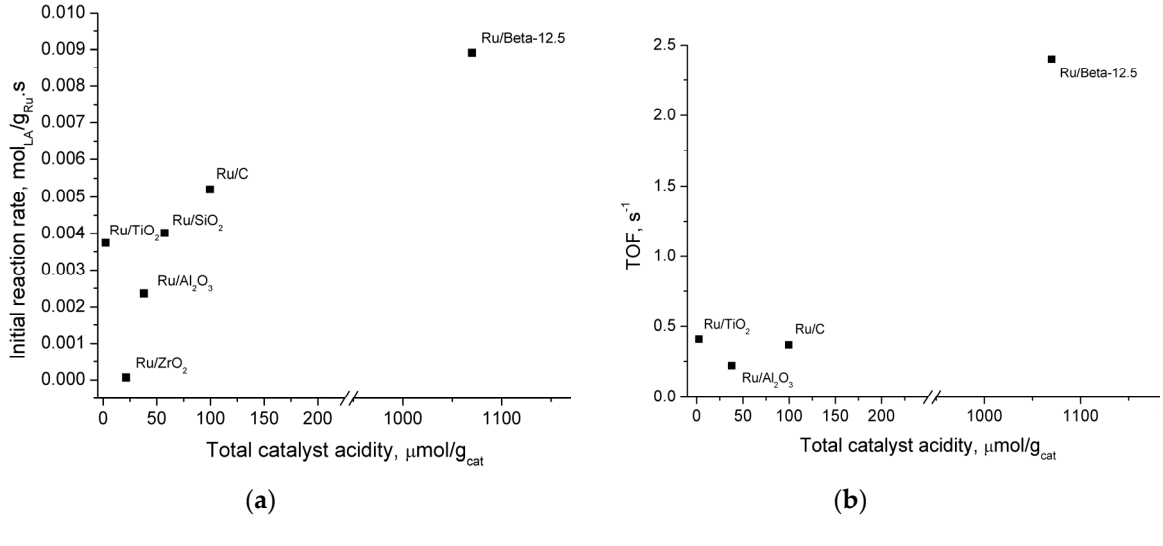

(**a**) (**b**)

Figure 7. Initial reaction rates and TOF (turnover frequency) values versus the total acidity of the catalysts for LA hydrogenations using supported Ru catalysts. (**a**) Initial reaction rate, (**b**) TOF.

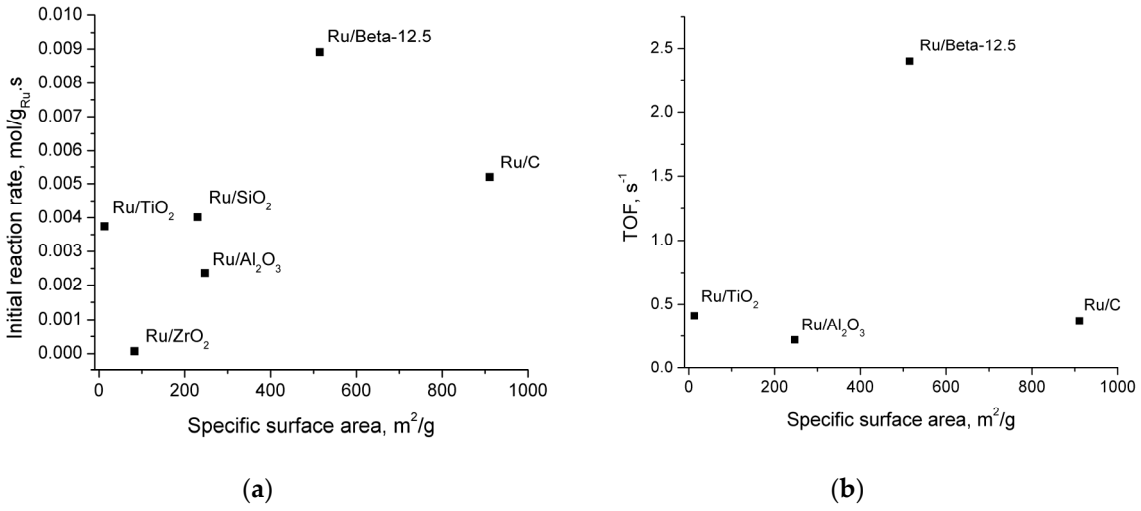

Figure 8. Initial reaction rate and TOF versus the specific surface areas of the catalysts for LA hydrogenations using supported Ru catalysts. (**a**) Initial reaction rate, (**b**) TOF.

Similar trends were observed when considering the effect of the micropore surface area on the initial activity and TOF (Figure 9). The initial reaction rate shows a maximum with regards to micropore surface area for Ru/Beta-12.5 but then reduces at higher areas for Ru/C. A similar observation was made by Ruppert et al. for Ru/TiO_2 catalysts [50]. Here, two catalyst were compared which were prepared using different procedures leading to different micropore volumes. The lowest activity was found for the catalyst with the highest micropore volume. The presence of small Ru nanoparticles in the TiO_2 micropores which are more difficult to reduce than larger particles and/or diffusion limitations of the reactants and products in the micropores were put forward as explanations for this observation.

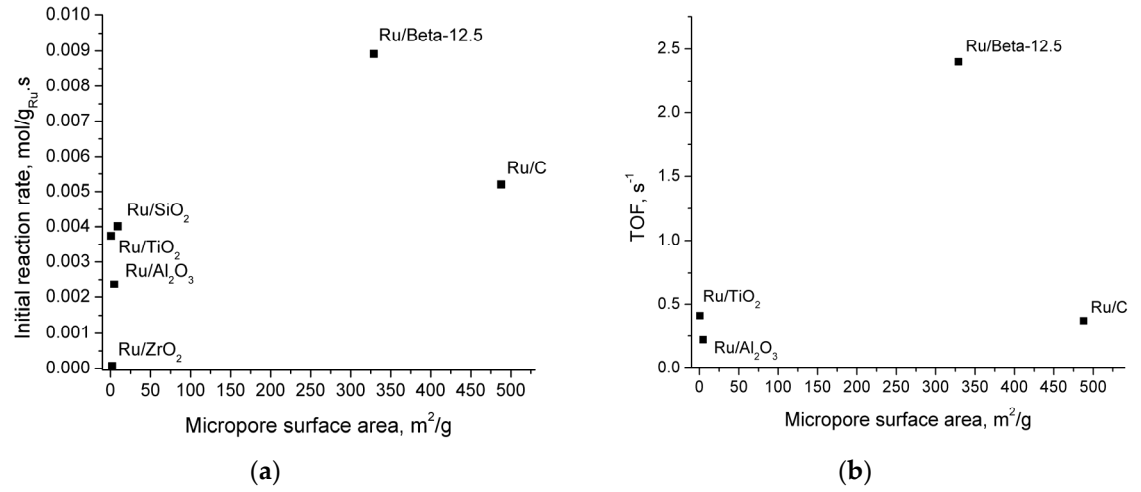

Figure 9. Initial reaction rate and TOF versus the micropore area of the catalysts for LA hydrogenations using supported Ru catalysts. (**a**) Initial reaction rate, (**b**) TOF.

However, the TOF values are rather insensitive to the micropore surface area, see Figure 9b for details, the only exception being the Ru/Beta-12.5 catalyst, which shows a by far higher TOF than the others.

Thus, we can conclude that relevant catalyst properties like Ru-nanoparticle size, support acidity and surface area (specific and micropore area) do not have a major effect on the TOF values for the hydrogenation of LA when using Ru/C, Ru/Al_2O_3 and Ru/TiO_2, which is indicative for a structure insensitive reaction. These findings are in line with the results obtained by Abdelrahman et al. for

Ru catalysts on C, Al_2O_3 and TiO_2 supports in a packed bed reactor [17]. In addition, related ketone hydrogenations, like glucose on Ru are also known to be structure insensitive [17,51]. However, the Ru/Beta-12.5 catalyst is a clear exception and the TOF for this catalyst is by far higher (factor 5, see Figure 9b) than for the others. This implies that the use of very acidic, highly porous supports leads to dramatic changes in support-Ru nanoparticle interactions and has a major (positive) impact on activity. The exact reason for the high activity of the Ru/Beta-12.5 catalyst needs to be established, e.g., by carrying out an extensive experimental study on LA hydrogenation using a wider range of zeolite based Ru catalysts with different acidity and other structural properties.

2.6. Catalyst Structure-Selectivity Relations

Analysis of the reaction mixtures only showed the presence of GVL and 4-HPA and over-hydrogenation products were absent. The ratio of 4-HPA/GVL for LA hydrogenations in water is typically a function of the batch time and in some cases the 4-HPA concentration shows a maximum (Figure 2) [8,19,49]. To gain insights in catalyst structure-selectivity relations, the [4-HPA]/[GVL] ratio after 2 h batch time was determined for the various catalysts (Figure 10). This shows that the [4-HPA]/[GVL] ratio is a function of the catalyst support (Figure 10).

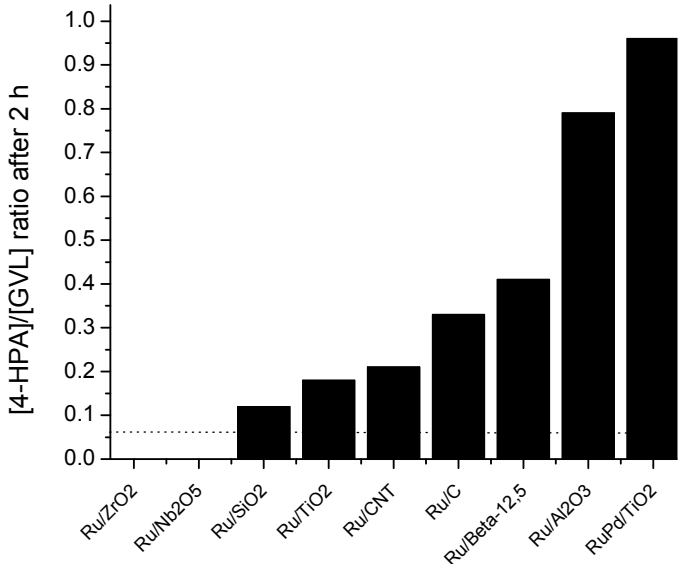

Figure 10. [4-HPA]/[GVL] ratio after 2 h batch time for various supported Ru catalysts. Dotted line-equilibrium value. Reaction conditions: 90 °C, 45 bar H_2, $C_{LA,0}$ = 0.6–0.7 mol/L, m_{cat} = 0.06 g, stirring rate = 2000 rpm.

The intramolecular esterification of 4-HPA to GVL is known to be an equilibrium reaction with an equilibrium constant (K = [4-HPA]/[GVL]) of about 0.05–0.06 at 90 °C [52]. As can be seen from Figure 10, equilibrium was not achieved within 2 h batch time for all catalytic runs. The highest [4-HPA]/[GVL] ratio was obtained for the bimetallic $RuPd/TiO_2$ catalyst (0.96), the lowest for Ru/SiO_2 (0.11). Due to low LA conversions (<2%) for Ru/ZrO_2 and Ru/Nb_2O_5, the [4-HPA]/[GVL] ratio could not be determined accurately and as such is not provided in Figure 10.

The [4-HPA]/[GVL] ratio is expected to be a function of the rate of hydrogenation versus the rate of intramolecular esterification. The former is Ru catalyzed, the esterification is expected to take place in the bulk solution and is known to be Brönsted acid catalyzed. When assuming that the rate of intramolecular esterification is mainly determined by acidity of the bulk solution and not by acidity of the surface, the ratio [4-HPA]/[GVL] is expected to be a function of the initial rate of the hydrogenation reaction, with higher initial reaction rates leading to higher [4-HPA]/[GVL] ratios. Indeed, the [4-HPA]/[GVL] ratio is proportional to the initial rate for the monometallic catalysts (Figure 11), the

only exception being the alumina catalyst (not shown in Figure 11). As such, the acidity of the support seems to play a minor role in the intramolecular esterification reaction. Further kinetic studies and modeling, beyond the scope of this study, will be required to draw more definite conclusions.

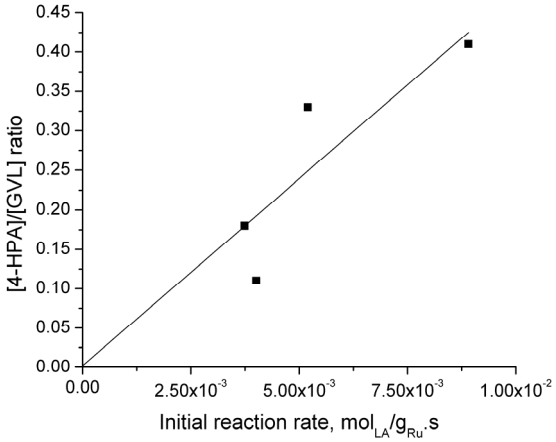

Figure 11. [4-HPA]/[GVL] ratio (concentration based) vs. initial reaction rate after 2 h batch time.

3. Experimental Section

3.1. Materials

Levulinic acid (purity >98%, less than 1 wt. % H_2O) and dioxane (purity >99%) were purchased from Acros Organics (Waltham, MA, USA). deuterium oxide (purity >99.9%) and urea (8 M) were from Sigma-Aldrich (Zwijndrecht, The Netherlands). Hydrogen and nitrogen (purity >99.9%) gas were from Linde Gas (Schiedam, The Netherlands).

$RuNO(NO_3)_3$ was supplied by Alfa Aesar (Ward Hill, MA, USA), $RUCl_3 \cdot xH_2O$ (35–40 wt. % Ru) and $PdCl_2$ (<99%) by Sigma-Aldrich (Zwijndrecht, The Netherlands). All chemicals were used without purification. Catalysts supports: TiO_2 (powder, anatase, ≥99%, average particle diameter as measured by scanning electron microscope (SEM) was 156 nm) and carbon nanotubes (multi-walled, outside diameter (O.D.) 6–9 nm length, 5 μm diameter, >95% carbon) were supplied by Sigma-Aldrich (Zwijndrecht, The Netherlands). γ-Al_2O_3 was from Albemarle Catalysts B.V. (Amsterdam, The Netherlands), ZrO_2 (monoclinic, Daiichi Kikenso RC-100) was purchased from Degussa (Essen, Germany), and SiO_2 (FUJI G6-5) was supplied by Fuji Silycia Chemical Ltd. (Kasugai, Japan). The Nb_2O_5 support was obtained by calcination of niobic acid (HY-340, CBMM) at 400 °C for 4 h under air flow; H-Beta-12.5 (CP814E, Si/Al = 12.5), from Zeolyst (Delfzijl, The Netherlands) was converted into the H-form by heating the samples to 120 °C for 1 h followed to 550 °C for 4 h.

A commercial Ru/C catalyst (1 wt. % Ru) was obtained from Evonik (Essen, Germany) (d_{10} = 5 μm, d_{50} = 25 μm, d_{90} = 75 μm). Ruthenium is well dispersed and, according to TEM measurements, the Ru nanoparticles have an average diameter of 1–2 nm.

3.2. Catalysts Preparation

Ru/CNT, Ru/TiO_2 and Ru/ZrO_2 (1 wt. % Ru) were prepared by a standardized procedure using a wet impregnation protocol. The support was dried (120 °C for 4 h in air) before use. The required amount of the precursor ($RuCl_3 \cdot xH_2O$) was dissolved in an excess of water at stirring (1100 rpm) for 30 min at 30 °C to obtain a homogeneous solution. The support was added to the precursor solution in small portions under stirring. Subsequently, the temperature was increased to 85 °C and kept at this value till complete water evaporation (after about 19 h). After the impregnation, the catalyst was reduced. Reduction was performed using a Micrometrics AutoChem II 2920 system (Norcross, GA,

USA) at 400 °C (heating rate 2 °C/min) in a N_2/H_2 atmosphere (10% H_2, total gas flow = 100 mL/min) for 4 h.

Ru/Al_2O_3 and Ru/SiO_2 (1 wt. % Ru) were prepared by a homogeneous deposition precipitation method as described by Toebes et al. [53]. A suspension (pH 2.0) of 1.25 g of support in demi water was heated up to 90 °C, and 0.39 g of urea and 0.03 g of $RuCl_3 \cdot xH_2O$ were added under vigorous stirring. The pH of the slurry was monitored continuously using a pH meter (Mettler-Toledo B.V., Tiel, The Netherlands). After 6 h the catalysts were filtered and washed thoroughly with demi water, dried at 120 °C, and calcined at 500 °C for 8 h (heating rate 4 °C/min).

Ru/Nb_2O_5 and Ru/Beta-12.5 (1 wt. % Ru) were prepared by wet impregnation using aqueous solutions of ruthenium nitrosyl nitrate ($RuNO(NO_3)_3$). After evaporation of the water, the catalysts were dried at 60 °C overnight, calcined at 500 °C for 4 h under N_2 (100 mL/min), followed by reduction at 400 °C, for 6 h, under a H_2 flow (80 mL/min).

The bimetallic $RuPd/TiO_2$ catalyst with equimolar metal ratios (1 wt. % of both metals) was synthesized via a modified wet impregnation method that involves the use of an excess of chloride anions [30]. The precursor ($RuCl_3 \cdot xH_2O$) was dissolved in deionized water to form an aqueous solutions with the preset ruthenium concentration. The $PdCl_2$ salt was dissolved in 0.5 M HCl under vigorous stirring and gentle warming to obtain an aqueous solution with the desired palladium concentration. This solution was slowly cooled and used as the palladium precursor. In a typical catalyst synthesis, the required amount of precursor solution was charged into a round bottomed flask equipped with a magnetic stirrer, after which the required amount of concentrated HCl (37.5%) was added. Subsequently, the volume of the precursor/HCl solution was diluted to 25 mL using water to obtain a final HCl concentration of 0.5 M in deionized water. The round bottom flask was submerged in a temperature controlled oil bath and the mixture was then agitated vigorously at 25 °C. To the stirred precursor solution, the required amount of the support was added very slowly with constant stirring at 25 °C over a period of 30 min. After complete support addition, the slurry was stirred vigorously and then the temperature was raised to 85 °C. The slurry was stirred at this temperature overnight until all water was evaporated. The solid powder obtained, denoted as the "dried sample", was grounded thoroughly and then reduced in a furnace at 450 °C under a flow of 5% H_2/He for 4 h.

3.3. Analysis

Nitrogen physisorption experiments were carried out using a Micromeritics ASAP 2020 (Micromeritics, Norcross, GA, USA) at −196.2 °C. The samples were degassed in vacuum at 200 °C for 10 h. The surface area was calculated using the standard BET method (SBET). The single point gas adsorption pore volume (VT) was calculated from the amount of gas adsorbed at a relative pressure of 0.98 in the desorption branch. The pore size distributions (PSD) were obtained from the Barrett-Joyner-Halenda (BJH) method using the adsorption branch of the isotherms. The mean pore size was taken as the position of the particle size distribution (PSD) maximum. The *t*-plot method was employed to quantify the micropore volume (V_m).

Temperature programmed desorption of ammonia (NH_3-TPD): NH_3-TPD measurements were performed using a Micrometrics AutoChem II 2920 system (Micromeritics, Norcross, GA, USA). Before TPD experiments, the catalysts (~50 mg) were pretreated at 300 °C at a heating rate of 10 °C/min for 30 min. Then the samples were cooled to 100 °C under a He flow. In the next step, the samples were saturated for 60 min in a flow of a gas containing 1% of NH_3 in He at 100 °C. Then, the samples were purged with a He flow until a constant baseline level was attained. TPD measurements were performed in the temperature range 100–600 °C at a rate of 10 °C/min using He as the carrier gas. The evolved NH_3 was detected by an on-line thermal-conductivity detector, calibrated by the peak area of known pulses of NH_3.

Transmission Electron Microscopy (TEM) measurements in bright field mode were conducted with a CM12 microscope (Philips, Eindhoven, The Netherlands), operating at 120 keV. Samples were made by ultra-sonication in ethanol and dropping the suspension onto carbon coated 400 mesh copper

grids. Images were taken on a slow scanning CCD camera (Philips, Eindhoven, The Netherlands). The metal particle distribution is calculated by measuring at least 100 particles with the software Nano Measurer 1.2 (Department of Chemistry, Fudan University, China).

X-ray fluorescence (XRF) measurements to determine the Ru loading on the supports were carried out using an XRF (Bruker S8 Tiger, Billerica, MA, USA) using a 4 kW Rhodium tube and 8 mm masks.

3.4. Catalytic Hydrogenation Experiments of LA

The hydrogenation reactions were performed in a stainless steel batch autoclave (100 mL, Parr Instrument Company, Moline, IL, USA). The mantle of the autoclave was equipped with electric heating rods and a cooling coil (using water) for proper temperature control. The reactor content was stirred using an overhead stirrer (Heidolph, RZR 2102 control, Saffron Walden, UK). The temperature and pressure were measured online with a Eurotherm 2208e (Eurotherm, Worthing, UK). The reactor was equipped with a dip-tube to allow for liquid sampling during the reaction.

LA dissolved in water (40 mL, 0.6 M) and catalyst (0.06 g, 2.0 wt. % on LA) were introduced in the autoclave. The stirrer was started (2000 rpm) and the system was flushed with nitrogen for 5 min. The mixture was heated to the desired temperature and subsequently hydrogen was admitted to the reactor to 45 bar. This moment is set as t = 0 min. During the reaction, hydrogen was admitted to the reactor to keep the pressure constant at 45 bar.

3.5. Definitions

The turnover frequency (TOF, s^{-1}) was calculated according to Equation (1).

$$TOF = \frac{R_0}{D_{Ru}} \tag{1}$$

where R_0 is the initial reaction rate (mol/mol_{Ru}·s, based on measured Ru loading of the catalyst) and D_{Ru} is the dispersion of Ru, which was calculated using Equation (2):

$$D_{Ru} = \frac{6 \times V_{Ru}}{a_{Ru} \times d_{Ru}} \tag{2}$$

where V_{Ru} is the volume occupied by a bulk Ru atom (0.01365 nm^3), a_{Ru} is an area per Ru atom (0.0635 nm^2) and d_{Ru} is the average diameter of a Ru particle (nm, taken from the TEM measurements).

The conversion of LA and the yield and selectivity for the products (4-HPA and GVL) were calculated according to Equations (3)–(5).

$$X_{LA} = \frac{C_{LA,\,0} - C_{LA}}{C_{LA,0}} \times 100\% \tag{3}$$

$$\begin{aligned} Y_{GVL} &= \frac{C_{LA,\,0} - C_{LA} - C_{4-HPA}}{C_{LA,0}} \times 100\% \\ Y_{4-HPA} &= \frac{C_{LA,\,0} - C_{LA} - C_{GVL}}{C_{LA,0}} \times 100\% \end{aligned} \tag{4}$$

$$S_i = \frac{Y_i}{X_{LA}} \times 100\% \tag{5}$$

where X_{LA} is the conversion of LA (mol. %); $C_{LA,0}$ the initial concentration of LA (mol/L); C_{LA} the concentration of LA at a certain time t (mol/L); Y_{GVL} the yield of GVL (mol. %); $Y_{4\text{-HPA}}$ the yield of 4-HPA (mol. %) and S_i the selectivity to GVL or 4-HPA (mol. %).

3.6. Determination of the Concentrations of LA, GVL and 4-HPA

The composition of a reaction mixture (LA, 4-HPA and GVL) was determined quantitatively by ^{1}H-NMR. This was shown to be the best method to quantify 4-HPA, which is difficult to determine using gas chromatography (GC) and high performance liquid chromatography (HPLC).

A sample (approximately 200 µL) was weighed, dissolved in D_2O and dioxane (S, internal standard, 10 µL) was added. All spectra were integrated using MestReNova software (10.0.1, Mestrelab, Santiago de Compostela, Spain, 2014). The number of moles of a component A in the sample was calculated using Equation (6):

$$mol_A = mol_s \times \left(\frac{Integral\ (component\ A)}{Integral\ (int.stand.)} \right) \times \frac{N_s}{N_A} \quad (6)$$

where N_A is the number of hydrogen atoms of the Nuclear Magnetic Resonance (NMR) peak used for the calculation (δ 2.1 ppm for LA (3 hydrogen atoms), δ 1.03 ppm for 4-HPA (3 hydrogen atoms), δ 1.3 ppm for GVL (3 hydrogen atoms)) and N_S is 8, being the number of hydrogen atoms of dioxane at δ 3.6 ppm. The concentrations of LA, GVL and 4-HPA in the samples were calculated using Equation (7).

$$C_A = \frac{N_A}{V_t} \times D_f \quad (7)$$

where V_t is the volume of the mixture in NMR tube and D_f the dilution factor, which was calculated as follows (Equation (8)):

$$D_f = \frac{mass\ of\ the\ sample\ in\ NMR\ tube + mass\ of\ D_2O + mass\ of\ internal\ standard}{mass\ of\ the\ sample\ in\ NMR\ tube} \quad (8)$$

3.7. Determination of the Initial Rates

The initial reaction rate was determined from the experimentally obtained concentration-time profiles using a procedure given by Fogler [54]. For this purpose, the concentration time profile was modeled using a higher order polynome. The initial rate was determined by differentiation of the polynome and setting the value for the time at zero.

4. Conclusions

A systematic experimental study on the catalytic hydrogenation of LA with a series of mono- and one bimetallic Ru catalysts (1 wt. % Ru) on various supports in water in a batch set up is reported. For all catalysts, GVL and 4-HPA were the main products and over hydrogenation product were not observed. The catalyst activity was shown to be a strong function of the support and the highest activity (TOF up to 2.4 mol_{LA}/mol_{Ru}·s at 90 °C and 45 bar H_2) was found for Ru/Beta-12.5. Relevant catalyst properties were determined (average Ru nanoparticle size, BET surface area, micropore area and total acidity) and used to determine correlations between catalyst activity and catalyst properties. It was found that TOF values of the catalysts are essentially independent of the catalyst properties for Ru/C, Ru/Al_2O_3 and Ru/TiO_2, indicative that the reaction is structure insensitive for these supports. However, the Ru/Beta-12.5 catalyst is a clear exception and the TOF for this catalyst is by far higher (factor 5) than for the others. Moreover, it was found that the [4-HPA]/[GVL] ratio at a certain batch time is a function of the catalyst support. This finding was rationalized by considering that the rate of hydrogenation of LA to 4-HPA, which is by far more dependent on the type of catalyst (and associated support) than the rate of the subsequent intramolecular esterification reaction of 4-HPA to GVL.

Supplementary Materials: The following are available online at www.mdpi.com/2073-4344/6/9/131/s1, Figure S1: Temperature programmed desorption of ammonia (NH_3-TPD) profiles of the various Ru-based catalysts (1 wt. % Ru), Figure S2: Parity plot for initial reaction rate (on actual Ru intake in g) and levulinic acid (LA) conversion after 2 h batch time for the various catalysts. Reaction conditions: 90 °C, 45 bar H_2, $C_{LA,0}$ = 0.6–0.7 mol/L, m_{cat} = 0.06 g, stirring rate = 2000 rpm.

Acknowledgments: This research has been performed within the framework of the CatchBio program, project 053.70.732. The authors gratefully acknowledge the financial support of the Smart Mix program of the Ministry of Economic Affairs and the Netherlands Ministry of Education, Culture and Science. The authors thank the members of the CatchBio User Committee for valuable suggestions and discussions, Pieter Bruijnincx and Wenhao Luo (University of Utrecht, The Netherlands) for some of the catalyst samples, Ramesh Kumar Chowdari

for NH3-TPD measurements and Tom Velthuizen and Shilpa Agarwal (catalytic processes and materials group, University of Twente, The Netherlands) for XRF measurements.

Author Contributions: A.P. synthesized catalysts, performed and analyzed the experiments, Z.T. performed TEM analysis, J.G.M.W. performed modeling calculations, H.J.H. supervised the research and together with A.P. prepared the manuscript.

Conflicts of Interest: The authors declare no conflict of interest.

References

1. Biddy, M.J.; Scarlata, C.; Kinchin, C. *Chemicals from Biomass: A Market Assessment of Bioproducts with Near-Term Potential*; National Renewable Energy Laboratory: Golden, CO, USA, 2016.
2. Yan, K.; Jarvis, C.; Gu, J.; Yan, Y. Production and catalytic transformation of levulinic acid: A platform for speciality chemicals and fuels. *Renew. Sustain. Energy Rev.* **2015**, *51*, 986–997. [CrossRef]
3. Morone, A.; Apte, M.; Pandey, R.A. Levulinic acid production from renewable waste resources: Bottlenecks, potential remedies, advancements and applications. *Renew. Sustain. Energy Rev.* **2015**, *51*, 548–565. [CrossRef]
4. Liguori, F.; Moreno-Marrodan, C.; Barbaro, P. Environmentally friendly synthesis of γ-valerolactone by direct catalytic conversion of renewable sources. *ACS Catal.* **2015**, *5*, 1882–1894. [CrossRef]
5. Manzer, L.E. Catalytic synthesis of α-methylene-γ-valerolactone: A biomass-derived acrylic monomer. *Appl. Catal. A Gen.* **2004**, *272*, 249–256. [CrossRef]
6. Al-Shaal, M.G.; Wright, W.R.H.; Palkovits, R. Exploring the ruthenium catalysed synthesis of γ-valerolactone in alcohols and utilisation of mild solvent-free reaction conditions. *Green Chem.* **2012**, *14*, 1260–1263. [CrossRef]
7. Michel, C.; Zaffran, J.; Ruppert, A.M.; Matras-Michalska, J.; Jędrzejczyk, M.; Grams, J.; Sautet, P. Role of water in metal catalyst performance for ketone hydrogenation: A joint experimental and theoretical study on levulinic acid conversion into gamma-valerolactone. *Chem. Commun.* **2014**, *50*, 12450–12453. [CrossRef] [PubMed]
8. Piskun, A.; van de Bovenkamp, H.H.; Rasrendra, C.B.; Winkelman, J.G.M.; Heeres, H.J. Kinetic modeling of levulinic acid hydrogenation to γ-valerolactone in water using a carbon supported ruthenium catalyst. *Appl. Catal. A* **2016**, *525*, 1–10. [CrossRef]
9. Yang, Y.; Gao, G.; Zhang, X.; Li, F. Facile fabrication of composition-tuned Ru-Ni bimetallics in ordered mesoporous carbon for levulinic acid hydrogenation. *ACS Catal.* **2014**, *4*, 1419–1425. [CrossRef]
10. Ding, D.; Wang, J.; Xi, J.; Liu, X.; Lu, G.; Wang, Y. High-yield production of levulinic acid from cellulose and its upgrading to γ-valerolactone. *Green Chem.* **2014**, *16*, 3846–3853. [CrossRef]
11. Castelijns, A.M.C.F.; Janssen, M.C.C.; Vaessen, H.W.L.M. Process to Produce Valerolactone from Levulinic Acid. U.S. Patent 20120329981A1, 27 December 2012.
12. Raspolli Galletti, A.M.; Antonetti, C.; De Luise, V.; Martinelli, M. A sustainable process for the production of γ-valerolactone by hydrogenation of biomass-derived levulinic acid. *Green Chem.* **2012**, *14*, 688–694. [CrossRef]
13. Yan, Z.P.; Lin, L.; Liu, S. Synthesis of γ-valerolactone by hydrogenation of biomass-derived levulinic acid over Ru/C catalyst. *Energy Fuels* **2009**, *23*, 3853–3858. [CrossRef]
14. Gong, Y.; Lin, L.; Yan, Z. Catalytic hydrogenation and oxidation of biomass-derived levulinic acid. *BioResources* **2011**, *6*, 686–699.
15. Luque, R.; Clark, J.H. Water-tolerant Ru-Starbon® materials for the hydrogenation of organic acids in aqueous ethanol. *Catal. Commun.* **2010**, *11*, 928–931. [CrossRef]
16. Hengne, A.M.; Kamble, S.B.; Rode, C.V. Single pot conversion of furfuryl alcohol to levulinic esters and γ-valerolactone in the presence of sulfonic acid functionalized ILs and metal catalysts. *Green Chem.* **2013**, *15*, 2540–2547. [CrossRef]
17. Abdelrahman, O.A.; Luo, H.Y.; Heyden, A.; Román-Leshkov, Y.; Bond, J.Q. Toward rational design of stable, supported metal catalysts for aqueous-phase processing: Insights from the hydrogenation of levulinic acid. *J. Catal.* **2015**, *329*, 10–21. [CrossRef]
18. Alonso, D.M.; Wettstein, S.G.; Dumesic, J.A. Gamma-valerolactone, a sustainable platform molecule derived from lignocellulosic biomass. *Green Chem.* **2013**, *15*, 584–595. [CrossRef]

19. Chalid, M. Levulinic Acid as a Renewable Source for Novel Polymers. Ph.D. Thesis, University of Groningen, Groningen, The Netherlands, 18 June 2012.
20. Xianlong, D.; Yongmei, L.; Jianqiang, W.; Yong, C.; Kangnian, F. Catalytic conversion of biomass-derived levulinic acid into γ-valerolactone using iridium nanoparticles supported on carbon nanotubes. *Chin. J. Catal.* **2013**, *34*, 993–1001.
21. Pan, X.L.; Fan, Z.L.; Chen, W.; Ding, Y.J.; Luo, H.Y.; Bao, X.H. Enhanced ethanol production inside carbon-nanotube reactors containing catalytic particles. *Nat. Mater.* **2007**, *6*, 507–511. [CrossRef] [PubMed]
22. Xiao, C.; Goh, T.-W.; Qi, Z.; Goes, S.; Brashler, K.; Perez, C.; Huang, W. Conversion of levulinic acid to γ-valerolactone over few-layer graphene-supported ruthenium catalysts. *ACS Catal.* **2016**, *6*, 593–599. [CrossRef]
23. Mai, E.F.; Machado, M.A.; Davies, T.E.; Lopez-Sanchez, J.A.; da Silva, V.T. Molybdenum carbide nanoparticles within carbon nanotubes as superior catalysts for γ-valerolactone production via levulinic acid hydrogenation. *Green Chem.* **2014**, *16*, 4092–4097. [CrossRef]
24. Lange, J.-P. Renewable feedstocks: The problem of catalyst deactivation and its mitigation. *Angew. Chem. Int. Ed.* **2015**, *54*, 13186–13197. [CrossRef] [PubMed]
25. Lange, J.-P.; Price, R.; Ayoub, P.M.; Louis, J.; Petrus, L.; Clarke, L.; Gosselink, H. Valeric biofuels: A platform of cellulosic transportation fuels. *Angew. Chem. Int. Ed.* **2010**, *49*, 4479–4483. [CrossRef] [PubMed]
26. Luo, W.; Deka, U.; Beale, A.M.; van Eck, E.R.H.; Bruijnincx, P.C.A.; Weckhuysen, B.M. Ruthenium-catalyzed hydrogenation of levulinic acid: Influence of the support and solvent on catalyst selectivity and stability. *J. Catal.* **2013**, *301*, 175–186. [CrossRef]
27. Luo, W.; Bruijnincx, P.C.A.; Weckhuysen, B.M. Selective, one-pot catalytic conversion of levulinic acid to pentanoic acid over Ru/H-ZSM-5. *J. Catal.* **2014**, *320*, 33–41. [CrossRef]
28. Bourne, R.A.; Stevens, J.G.; Ke, J.; Poliakoff, M. Maximising opportunities in supercritical chemistry: The continuous conversion of levulinic acid to γ-valerolactone in CO_2. *Chem. Commun.* **2007**, 4632–4634. [CrossRef] [PubMed]
29. Manzer, L.E.; Hutchenson, K.W. Production of 5-Methylbutyrolactone from Levulinic Acid. U.S. Patent 20040254384A1, 20 March 2003.
30. Luo, W.; Sankar, M.; Beale, A.M.; He, Q.; Kiely, C.J.; Bruijnincx, P.C.A.; Weckhuysen, B.M. High performing and stable supported nano-alloys for the catalytic hydrogenation of levulinic acid to γ-valerolactone. *Nat. Commun.* **2015**, *6*, 6540–6550. [CrossRef] [PubMed]
31. Sudhakar, M.; Kantam, M.L.; Jaya, V.S.; Kishore, R.; Ramanujachary, K.V.; Venugopal, A. Hydroxyapatite as a novel support for Ru in the hydrogenation of levulinic acid to γ-valerolactone. *Catal. Commun.* **2014**, *50*, 101–104. [CrossRef]
32. Yao, Y.; Wang, Z.; Zhao, S.; Wang, D. A stable and effective Ru/polyethersulfone catalyst for levulinic acid hydrogenation to γ-valerolactone in aqueous solution. *Catal. Today* **2014**, *234*, 245–250. [CrossRef]
33. Heeres, H.; Handana, R.; Chunai, D.; Rasrendra, C.B.; Girisuta, B.; Heeres, H.J. Combined dehydration/(transfer)-hydrogenation of C6-sugars (D-glucose and D-fructose) to γ-valerolactone using ruthenium catalysts. *Green Chem.* **2009**, *11*, 1247–1255. [CrossRef]
34. Raspolli Galletti, A.M.; Antonetti, C.; Ribechini, E.; Colombini, M.P.; Nassi o Di Nasso, N.; Bonari, E. From gient reed to levulinic acid and gamma-valerolactone: A high yield catalytic route to valeric biofuels. *Appl. Energy* **2013**, *102*, 157–162. [CrossRef]
35. Son, P.A.; Nishimura, S.; Ebitani, K. Production of γ-valerolactone from biomass-derived compounds using formic acid as a hydrogen source over supported metal catalysts in water solvent. *RSC Adv.* **2014**, *4*, 10525–10530. [CrossRef]
36. Lee, M.; Seo, Y.; Shin, H.S.; Jo, C.; Ryoo, R. Anatase TiO_2 nanosheets with surface acid, sites for Friedel-Crafts alkylation. *Microporous Mesoporous Mater.* **2016**, *222*, 185–191. [CrossRef]
37. Kaplan, R.; Erjavec, B.; Dražić, G.; Grdadolnik, J.; Pintar, A. Simple synthesis of anatase/rutile/brookite TiO_2 nanocomposite with superior mineralization potential for photocatalytic degradation of water pollutants. *Appl. Catal. B* **2016**, *181*, 465–474. [CrossRef]
38. Lin, B.; Wei, K.; Ma, X.; Lin, J.; Ni, J. Study of potassium promoter effect for Ru/AC catalysts for ammonia synthesis. *Catal. Sci. Technol.* **2013**, *3*, 1367–1374. [CrossRef]
39. Deng, W.; Tan, X.; Fang, W.; Zhang, Q.; Wang, Y. Conversion of cellulose into sorbitol over carbon nanotube-supported ruthenium catalyst. *Catal. Lett.* **2009**, *133*, 167–174. [CrossRef]

40. Mierczynski, P.; Vasilev, K.; Mierczynska, A.; Maniukiewicz, W.; Ciesielski, R.; Rogowski, J.; Szynkowska, I.M.; Trifonov, A.Y.; Dubkov, S.V.; Gromov, D.G.; et al. The effect of gold on modern bimetallic Au-Cu/MWCNT catalysts for the oxy-steam reforming of methanol. *Catal. Sci. Technol.* **2016**, *6*, 4168–4183. [CrossRef]
41. Kumar, V.P.; Beltramini, J.N.; Priya, S.S.; Srikanth, A.; Bhanuchander, P.; Chary, K.V.R. Catalytic functionalities of nano Ru catalysts supported on TiO_2-ZrO_2 mixed oxide for vapor phase hydrogenolysis of glycerol to propanediols. *Appl. Petrochem. Res.* **2016**, *6*, 73–87. [CrossRef]
42. Leo, I.M.; Granados, M.L.; Fierro, J.L.G.; Mariscal, R. Sorbitol hydrogenolysis to glycols by supported ruthenium catalysts. *Chin. J. Catal.* **2014**, *35*, 614–621. [CrossRef]
43. Wang, M.; Yang, H.; Xie, Y.; Wu, X.; Chen, C.; Ma, W.; Dong, Q.; Hou, Z. Catalytic transformation of glycerol to 1-propanol by combining zirconium phosphate and supported Ru catalysts. *RCS Adv.* **2016**, *6*, 29769–29778. [CrossRef]
44. Serp, P.; Corrias, M.; Kalck, P. Carbon nanotubes and nanofibers in catalysis. *Appl. Catal. A* **2003**, *253*, 337–358. [CrossRef]
45. Martinez-Franco, R.; Paris, C.; Martinez-Armero, M.E.; Martinez, C.; Moliner, M.; Corma, A. High-silica nanocrystalline Beta zeolites: Efficient synthesis and catalytic application. *Chem. Sci.* **2016**, *7*, 102–108. [CrossRef]
46. López, T.; Herrera, L.; Mendez-Vivar, J.; Bosch, P.; Gómez, R.; Gonzalez, R.D. Support effect in ruthenium sol-gel catalysts on silica and alumina. *J. Non Cryst. Solids* **1992**, *147–148*, 773–777. [CrossRef]
47. Sun, G.; Xu, A.; He, Y.; Yang, M.; Du, H.; Sun, C. Ruthenium catalysts supported on high-surface-area zirconia for the catalytic wet oxidation of *N*,*N*-dimethyl formamide. *J. Hazard. Mater.* **2008**, *156*, 335–341. [CrossRef] [PubMed]
48. Okal, J. Characterization and thermal stability of ruthenium nanoparticles supported on γ-alumina. *Catal. Commun.* **2010**, *11*, 508–512. [CrossRef]
49. Abdelrahman, O.A.; Heyden, A.; Bond, J.Q. Analysis of kinetics and reaction pathways in the aqueous-phase hydrogenation of levulinic acid to form γ-valerolactone over Ru/C. *ACS Catal.* **2014**, *4*, 1171–1181. [CrossRef]
50. Ruppert, A.M.; Grams, J.; Jędrzejczyk, M.; Matras-Michalska, J.; Keller, N.; Ostojska, K.; Sautet, P. Titania-supported catalysts for levulinic acid hydrogenation: Influence of support and its impact on γ-valerolactone yield. *ChemSusChem.* **2015**, *8*, 1538–1547. [CrossRef] [PubMed]
51. Maris, E.P.; Ketchie, W.C.; Vladimir, O.; Davis, R.J. Metal particle growth during glucose hydrogenation over Ru/SiO_2 evaluated by X-ray absorption spectroscopy and electron microscopy. *J. Phys. Chem. B* **2006**, *110*, 7869–7876. [CrossRef] [PubMed]
52. Piskun, A.; van de Bovenkamp, H.H.; Pidko, E.; Heeres, H.J. Experimental and modeling studies on the equilibrium reaction between gamma-valerolactone and 4-hydroxypentanoic acid in water. 2016. Manuscript in preparation.
53. Toebes, M.L.; Prinsloo, F.F.; Bitter, J.H.; van Dillen, A.J.; de Jong, K.P. Influence of oxygen-containing surface groups on the activity and selectivity of carbon nanofiber-supported ruthenium catalysts in the hydrogenation of cinnamaldehyde. *J. Catal.* **2003**, *214*, 78–87. [CrossRef]
54. Fogler, H.S. *Elements of Chemical Reaction Engineering*, 4th ed.; Prentice Hall: Upper Saddle River, NJ, USA, 2006.